THE UNIVERSITY OF KANSAS SPACE TECHNOLOGY CENTER
Raymond Nichols Hall
2291 Irving Hill Drive—Campus West Lawrence, Kansas 66045
Telephone:

A THEORY OF SEA SCATTER AT LARGE INCIDENT ANGLES

Remote Sensing Laboratory
RSL Technical Report 254-4

A. K. Fung
H. L. Chan

October, 1975

Approved for public release; distribution unlimited

Prepared for:
National Aeronautics and Space Administration
Lyndon B. Johnson Space Center
Houston, Texas

Organization Full Name:	The University of Kansas Center for Research, Inc. 2291 Irving Hill Drive – West Campus Lawrence, Kansas 66045
Title of Investigation:	A Joint Meteorological, Oceanographic, and Sensor Evaluation Program for Experiment S-192 on Skylab
Title of Report:	A Theory of Sea Scatter at Large Incident Angles
Period Covered:	N.A.
EREP Investigation:	EREP #550
NASA Contract:	NAS 9-13642
Principal Investigator:	Prof. W. J. Pierson, CUNY
Co-Principal Investigator:	Prof. R. K. Moore, KU
Date Written:	October, 1975
Monitor and Address:	Mr. Zach H. Byrns / TF6 Principal Investigation Management Office NASA Lyndon B. Johnson Space Center Houston, Texas 77058
Type of Report:	Advance Report of Significant Results

A THEORY OF SEA SCATTER AT LARGE INCIDENT ANGLES

A. K. Fung
H. L. Chan

ABSTRACT

A theory for sea scatter at large incident angles ($\theta \geq 30^{\circ}$) is developed using a two-scale roughness model. The assumed small scale waves are to satisfy the small perturbation assumptions and the large scale waves to satisfy the physical optics approximations. Measured sea surface slope density and sea spectra reported by oceanographers are incorporated into the theory to explain effects of incident angle, polarization, frequency, wind speed and anisotropic characteristics of the sea surface.

It is observed that the increase of the backscattering coefficients with the wind is due primarily to the growth of the sea spectrum and, to a lesser extent, to the interaction between the two scales of roughness. This interaction effect is also the cause of the shift of the minimum of the scattering coefficient around the crosswind direction towards the downwind direction. The difference between the upwind and the crosswind observations is the result of the anisotropic characteristics in the sea spectrum, while the difference between the upwind and downwind observations is the consequence of the skewness in the slope probability density function of the large scale waves. Comparison with some experimental data shows satisfactory agreements.

LIST OF FIGURES

1.0 INTRODUCTION

It has been generally agreed[1-5] that the scattering properties of the sea surface can be explained reasonably well in terms of a two-scale roughness model where the small scale waves are assumed to satisfy the small perturbation assumptions while the large scale waves are to satisfy the Kirchhoff approximation. The basic approach is to use the first order result of the small perturbation method to compute the scattering coefficient due to small scale waves and to account for the tilting effect of the large scale waves by averaging this scattering coefficient over the slope distribution of the large scale waves. This averaged scattering coefficient is such that for near grazing incidence the vertically polarized scattering coefficient so computed is always larger than the corresponding horizontally polarized coefficient. Since recent experimental data[5] indicate that there are cases where the converse is true, it is clear that such a theory may not be applicable near grazing incidence. However, for incident angles between 30° and 80° the theory is expected to be valid.

2.0 THE SCATTER THEORY

Many authors[1,2,6] have shown that for a slightly rough surface which satisfies the small perturbation assumption, the backscattering coefficient is given by (Figure 1)

$$\sigma_{pp}(\theta,\phi) = 8 K^4 \sigma_1^2 |\alpha_{pp}|^2 W(\theta,\phi) \qquad (1)$$

where for horizontal polarization, p=h and

$$\alpha_{hh} = \cos^4\theta |R_h|^2$$

R_h is the Fresnel reflection coefficient for horizontal polarization and for vertical polarization, p=v and

$$\alpha_{vv} = Rv \cos^2\theta + (k'^2-k^2) Tv^2 \sin^2\theta/(2k'^2)$$

where Rv and Tv are the Fresnel reflection and transmission coefficients for vertical polarization. In α_{pp}, k is the wave number in air; k' is the wave number in sea water and θ is the angle of incidence. $W(\theta,\phi)$ is the normalized anisotropic sea spectrum and σ_1^2 is the variance of the small scale sea waves. To include the tilting effect of the large scale waves, it is necessary to average σ_{pp} over the slope distribution (as viewed by the receiver) of the large scale waves. Thus, the incident angle in (1) becomes the local incident angle (denoted by θ' in (2)) and the averaged scattering coefficient is (Figure 1)

$$\sigma^{\circ}_{pp}\ (\Theta,\phi) = \int_{-\infty}^{\infty}\int_{-\cot\theta}^{\infty} \sigma_{pp}(\Theta',\phi)\ P_{\theta}\ (Zx',\ Zy')\ dZx dZy \qquad (2)$$

Note that the local incident angle θ' is a function of the incident angle θ and the surface slopes, Zx and Zy. In (2) P_{θ} (Zx', Zy') is the slope distribution of the large scale waves as viewed at an incident angle θ and is defined in the prime coordinates whose x' – axis is parallel to the wind direction. It is assumed that the plane of incidence is the XZ plane and that the angle between the x – axis and the x' – axis is ϕ so that an upwind observation occurs when $\phi = 0$.

It is important to note that the probability of occurrence of a slope on a given surface varies with the direction of observation. To illustrate this point consider a piece of one-dimensional surface depicted in Figure 2. The probability of occurrence for slope Zx_2 when viewed from an angle θ is

$$P_{\theta}\ (Zx_2) = \frac{\ell_2\hat{n}_2\cdot\hat{a}}{(\ell_1\hat{n}_1+\ell_2\hat{n}_2+\ell_3\hat{n}_3)\cdot\hat{a}} \equiv \frac{\ell_2\hat{n}_2\cdot\hat{a}}{L_{\theta}}$$

where $\hat{a} = \hat{z}\cos\theta - \hat{x}\sin\theta$ and $\hat{n}_i$ are unit normal vectors to the surface. On the other hand, it becomes

$$P\ (Zx_2) = \frac{\ell_2\hat{n}_2\cdot\hat{z}}{(\ell_1\hat{n}_1+\ell_2\hat{n}_2+\ell_3\hat{n}_3)\cdot\hat{z}} \equiv \frac{\ell_2\hat{n}_2\cdot\hat{z}}{L}$$

when viewed from the vertical. Hence,

$$P_\theta\ (Zx_2) = \frac{L}{L_\theta}(\cos\theta + Zx_2 \sin\theta)\ \ P\ \ (Zx_2)$$

Since the total probability must be one, the ratio L/L_θ can be determined by this condition. Similarly, for two-dimensional surface, the slope probability density function viewed from an angle θ can be shown to relate to the slope probability density function viewed from the vertical as

$$P_\theta\ (Zx', Zy') = (1 + Zx' \tan\theta)\ P\ (Zx', Zy') \qquad (3)$$

Attempts to measure $P(Zx', Zy')$ for the ocean surface were made by Cox and Munk[7] and for a slick sea surface (one which excludes small scale waves) it was reported that

$$P(Zx', Zy') = \frac{F(Zx', Zy')}{2\pi\sigma_u\ \ \sigma_c}\ \ \exp\left[-\frac{Zx'^2}{2\sigma_u^{\,2}} - \frac{Zy'^2}{2\,\sigma_c^{\,2}}\right]$$

where

$$F(Zx', Zy') = 1 - \frac{C_{21}}{2}\left(\frac{Zy'^2}{\sigma_c^{\,2}} - 1\right)\frac{Zx'}{\sigma_u} - \frac{C_{03}}{6}\left(\frac{Zx'^3}{\sigma_u^{\,3}} - \frac{3Zx'}{\sigma_u}\right)$$
$$+ \frac{C_{40}}{24}\left(\frac{Zy'^4}{\sigma_c^{\,4}} - 6\frac{Zy'^2}{\sigma_c^{\,2}} + 3\right) + \frac{C_{22}}{4}\left(\frac{Zy'^2}{\sigma_c^{\,2}} - 1\right)\left(\frac{Zx'^2}{\sigma_u^{\,2}} - 1\right)$$
$$+ \frac{C_{04}}{24}\left(\frac{Zx^4}{\sigma_u^{\,4}} - 6\ \frac{Zx'^2}{\sigma_u^{\,2}} + 3\right).$$

Each constant in $F(Zx', Zy')$ was reported by Cox and Munk to lie within a range of values. Further study by other oceanographers may lead to more refined estimates. For the purpose of illustration only one value is chosen for each constant as follows:

$$\sigma_u^2 = 0.007 + 0.78 \times 10^{-3} U$$
$$\sigma_c^2 = 0.005 + 0.84 \times 10^{-3} U$$
$$C_{21} = 0 \qquad C_{03} = -0.05 \qquad C_{40} = 0.36$$
$$C_{22} = 0.1 \qquad\qquad\qquad C_{04} = 0.26$$

In the expressions for σ_u^2 and σ_c^2, U is the wind speed in meter per second at an altitude of 41 feet above the sea horizon. The relations between the surface slopes in the primed and unprimed coordinates are as follows (see Figure 1):

$$Zx' = Zx \cos\phi + Zy \sin\phi$$
$$Zy' = Zy \cos\phi - Zx \sin\phi$$

3.0 THE SEA SPECTRUM

The spectrum for the small scale waves to be used in this paper is a modification of Pierson and Stacy's sea spectrum[8]. The major change proposed by Pierson[9] is that their spectrum expression for the capillary region has been replaced by the one reported by Mitsuyasu and Honda[10]. The important characteristics to be noted in this spectral model are (1) the spectrum grows with the wind; (2) in the capillary region the larger the K number the faster is the growth; and (3) this model is valid to about 38 knots[8]. In accordance with Mitsuyasu and Honda, their model can be valid to friction velocity as high as 33m/sec at 10 meters above the sea horizon. Thus, the theory may be valid to higher wind speed than the 38 knots when operating frequency is such that only their portion of the sea spectrum is the significant contributor. Also, it should be noted that the definition of $W(\theta, \phi)$ in (4) is not the same as the one used by Pierson and Stacy

in that $W(\theta,\phi)$ is defined for all ϕ between 0 and 2π. If Pierson and Stacy's sea spectrum is extended to cover the same angular range, it can be shown that the complete expression of the modified directional sea spectrum is as follows:

$$\sigma_1^2 W(K,\phi) = S(K)\,(1 + a_0 \cos 2\phi) \;/\; K \qquad (4)$$

where higher order terms in ϕ has been ignored; a_0 is the only unknown parameter not yet specified; and where

$$S(K) = S_i(K), \quad K_{i-1} < K < K_i$$

$$S_1(K) = \frac{a}{K^3} \exp -\left[\frac{0.74g^2}{K^2 U(U_*)^4}\right], \quad 0 < K < K_1 = \frac{K_2 U_*^2 m}{U_*^2}$$

$$S_2(K) = a\, K_1^{-1/2} K^{-5/2}, \quad K_1 < K < K_2 = 0.359$$

$$S_3(K) = S_4(K_3)\,(K/K_3)^q, \quad K_2 < K < K_3 = 0.942$$

$$S_4(K) = 0.875\,(2\pi)^{\rho_1 - 1} \frac{g + 3gK^2/13.1769}{(gK + gK^3/13.1769)^{(\rho_1 + 1\,1/2)}} \quad K_3 < K < K_4$$

$$S_5(K) = 1.473 \times 10^{-4} U_*^3 K_m^6 K^{-9}, \quad K_4 < K < \infty$$

K_4 can be found numerically by settings $S_4(K_4)$ equal to $S_5(K_4)$.

U_* = friction velocity, $U_* > U_{*m}$

$K_m = (13,1769)^{1/2}$

$q = \left[\log_{10} S_2(K_2)/S_4(K_3)\right] \Big/ \log_{10}(K_2/K_3)$

$\rho_1 = 5.0 - \log_{10} U_*$

$z_o = 0.684/U_* + 4.28 \times 10^{-5} U_*^2 - 4.43 \times 10^{-2}$

$U(U_*) = (U_*/0.4) \ln(z/z_o)$ cm/sec

$a = 4.05 \times 10^{-3}$

$g = 980$ cm/sec^2

$U_{*m} = 12$ cm/sec

4.0 THEORETICAL RESULTS AND COMPARISON WITH EXPERIMENTAL DATA

Upon combining (1) (3) and (4) and substituting into (2), we obtain for the backscattered case

$$\sigma_{pp}^{\circ}(\theta,\phi) = \int_{-\infty}^{\infty}\int_{-\cot\theta}^{\infty} 4K\,|\alpha_{pp}|^2 \left[(1+a_o\cos 2\phi)/\sin\theta'\right] S(2k\sin\theta')\,(1+Zx'\tan\theta)\,p(Zx', Zy')\,dZx\,dZy \qquad (5)$$

In (5) the unknown constant a_o can be estimated by plotting σ° versus ϕ curves and comparing these curves with experimental data. In all Figures 3-8 wind speeds are computed at 19.5 m above the sea horizon. In Figure 3 and 4 σ° versus ϕ curves are plotted for two different wind speeds at $\theta = 30^\circ$ and $\theta = 60^\circ$ and for various choices of a_o. At $\theta = 30^\circ$ only vertically polarized curves are shown since the difference in σ° due to polarization is small. At 60° the difference in σ° becomes significant and hence σ for both polarizations are shown. The data points in Figure 3 and 4 were obtained from reference 11.

In Figure 4a, the data indicated by circles were taken for ϕ between 0° and 180° and the squares denote data for ϕ between 180° and 360°. The square-data were folded back under symmetry assumptions to compare with the circle data. It follows from 3a and 4a that $a_o \approx 0.3$ at 12 knots and $a_o \approx 0.40$ at 30 knots. It is also noted from these curves that two local maxima occur around the upwind and the downwind directions and a local minimum occurs near the crosswind direction. In addition, the location of σ° minimum tends to shift towards the downwind direction as wind speed or incident angle increases. This effect is most significant for horizontal polarization. The fact that σ° upwind is larger than σ° downwind is due to the skewness in the slope density function, $P_\theta(Zx', Zy')$.

In Figure 4b and 4c σ° versus ϕ curves using only the first order small perturbation theory are also plotted. Results correspond to the case when there is no tilting effect due to large scale waves. Comparison between these curves and those obtained by using (5) indicates that the use only of the first order small perturbation theory fails to account for (i) the difference between the upwind and the downwind scattering coefficients (ii) the possible shift of the minimum of σ° towards downwind and (iii) the true σ° values around the crosswind direction which are higher due to the interaction between the two scales of roughness.

With a_o chosen to be 0.3, 0.4 and 0.50 at wind speeds at 6.2, 12.6 and 18 m/sec respectively, σ° versus wind speed curves are computed for two different frequencies, polarizations and incident angles as shown in Figure 5 through Figure 8. In general, upwind scattering coefficient, σ°_U, is found to increase faster with wind speed than the downwind coefficient, σ°_D, which in turn increases faster than the crosswind coefficient, σ°_C. All three scattering coefficients are found to increase faster with the wind speed as either the incident frequency or the incident angle increases. The rate of increase of the scattering coefficients with wind speed is larger for horizontal polarization than for vertical polarization. For incident angles beyond 60° the level differences between these coefficients also increases with wind speed. When the theoretical σ° versus wind speed result is fitted over the wind speed range from 12.5 knots to 25.4 knots by the equation $\sigma^\circ = AU^\gamma$ where A is a constant; U is wind speed and γ is the wind speed power coefficient, a table for γ can be constructed for different frequencies, directions, polarizations, and incident angles. Such a table for two different frequencies is given below.

DIRECTION	POLARIZATION	THEORETICAL γ					
		8.9 GHz			13.9 GHz		
		INCIDENT ANGLES			INCIDENT ANGLES		
		40°	50°	60°	40°	50°	60°
U	VV	1.40	1.48	1.55	1.63	1.80	1.81
D		1.38	1.45	1.49	1.6	1.75	1.75
C		1.07	1.16	1.2	1.3	1.3	1.45
U	HH	1.47	1.62	1.73	1.70	1.93	2.01
D		1.42	1.51	1.56	1.65	1.82	1.83
C		1.11	1.26	1.36	1.34	1.43	1.64

To see that the wind dependence predicted from the present theory is in general agreement with experimental data, a table showing the γ values reported by Jones, et al.,[11] and Moore, R. K., et al[12] is reproduced below. Comparison between these tables shows that general agreement is, indeed, obtained for the 13.9 GHz data.

DIRECTION	POLARIZATION	γ					
		NRL (8.9 GHz)		AAFE (13.9 GHz)		SKYLAB S-193 (13.9 GHz)	
		INCIDENT ANGLE		INCID. NI ANGLE		INCIDENT ANGLE	
		40°	50°	40°	50°	40°	50°
U	VV	0.66	0.73	1.77	1.66	1.68	1.82
D		0.80	0.80	1.62	1.55		
C				1.52	1.51		
U	HH	0.87	1.03	1.93	1.93	1.83	2.11
D		1.04	1.30	1.97	1.96		
C				1.46	1.48		

5.0 CONCLUSION

A growing sea spectrum[9,10] and a two-scale roughness model[1-5] recommended by many investigators for studying radar sea scatter have been extended to include anisotropic characteristics of the sea surface. From such a theory, the following observations may be made:

(1) In the σ^o versus ϕ curves the local minimum occurs around the crosswind direction and tends to shift towards the downwind side as the incident angle increases. This is particularly true for horizontal polarization.

(2) Stronger wind dependence occurs at larger incident angles and higher frequencies.

(3) The wind dependence of σ^o upwind is stronger than σ^o downwind which in turn is stronger than σ^o crosswind.

(4) Major factors contributing to anisotropy are the anisotropic sea spectrum and the nonzero mean slope in the large-scale-wave slope density function defined with respect to the plane perpendicular to the look direction.

REFERENCES

1. Wright, J. W., "A New Model for Sea Clutter", IEEE Trans. on Antennas and Propagation, v. AP-16, no. 2, March, 1968, pp. 217-223.

2. Chan, H. L. and A. K. Fung, "Backscattering From a Two-Scale Rough Surface With Application to Radar Sea Return", NASA Contractor Report CR-2327, November, 1973.

3. Bass, F. G., I. M. Fuks, A. I. Kalmykov, I. E. Ostrovsky and A. D. Rosenberg, "Very High Frequency Radiowave Scattering by a Disturbed Sea Surface", IEEE Trans. on Antennas and Propagation, v. AP-16, no. 5, September, 1968, pp. 560-568.

4. Wu, S. T. and A. K. Fung, "A Noncoherent Model for Microwave Emissions and Backscattering From the Sea Surface", J. Geophysical Res., v. 77, no. 30, pp. 5917-5929, October, 1972.

5. Long, M. W., "On a Two-Scatterer Theory of Sea Echo", IEEE Trans. on Antennas and Propagation, v. AP-22, no. 5, September, 1974.

6. Valenzuela, G. R., "Depolarization of EM Waves by Slightly Rough Surfaces", IEEE, v. AP-15, no. 4, July, 1967, pp. 552-557.

7. Cox, C. and W. Munk, "Measurement of the Roughness of the Sea Surface From Photographs of the Sun Glitter", J. Opt. Soc. Am., v. 44, no. 11, pp. 838-850, November, 1954.

8. Pierson, W. J. and R. A. Stacy, "The Elevation, Slope and Curvature Spectra of a Wind Roughened Sea", NASA Contractor Report CR-2247, 1973.

9. Pierson, W. J., "The Theory and Application of Ocean Wave Measuring Systems at and Below the Sea Surface, On the Land, From Aircraft and From Spacecraft", Contractor Report, Goddard Space Flight Center (NAS 5-22041), 1975.

10. Mitsuyasu, H. and T. Honda, "The High Frequency Spectrum of Wind-Generated Waves", J. Oceanographical Soc. of Japan, v. 30, no. 4, August, 1974, pp. 185-198.

11. Jones, W. L. et al., "Microwave Scattering From the Ocean Surface", MIT-S International Microwave Symposium, Palo Alto, California, May, 1975.

12. Moore, R. K. et al., "Skylab S-193 Radscat Microwave Measurements of Sea Surface Winds", Earth Resources Survey Symposium, June 8-13, 1975, Houston, Texas, Office of Applications of NASA.

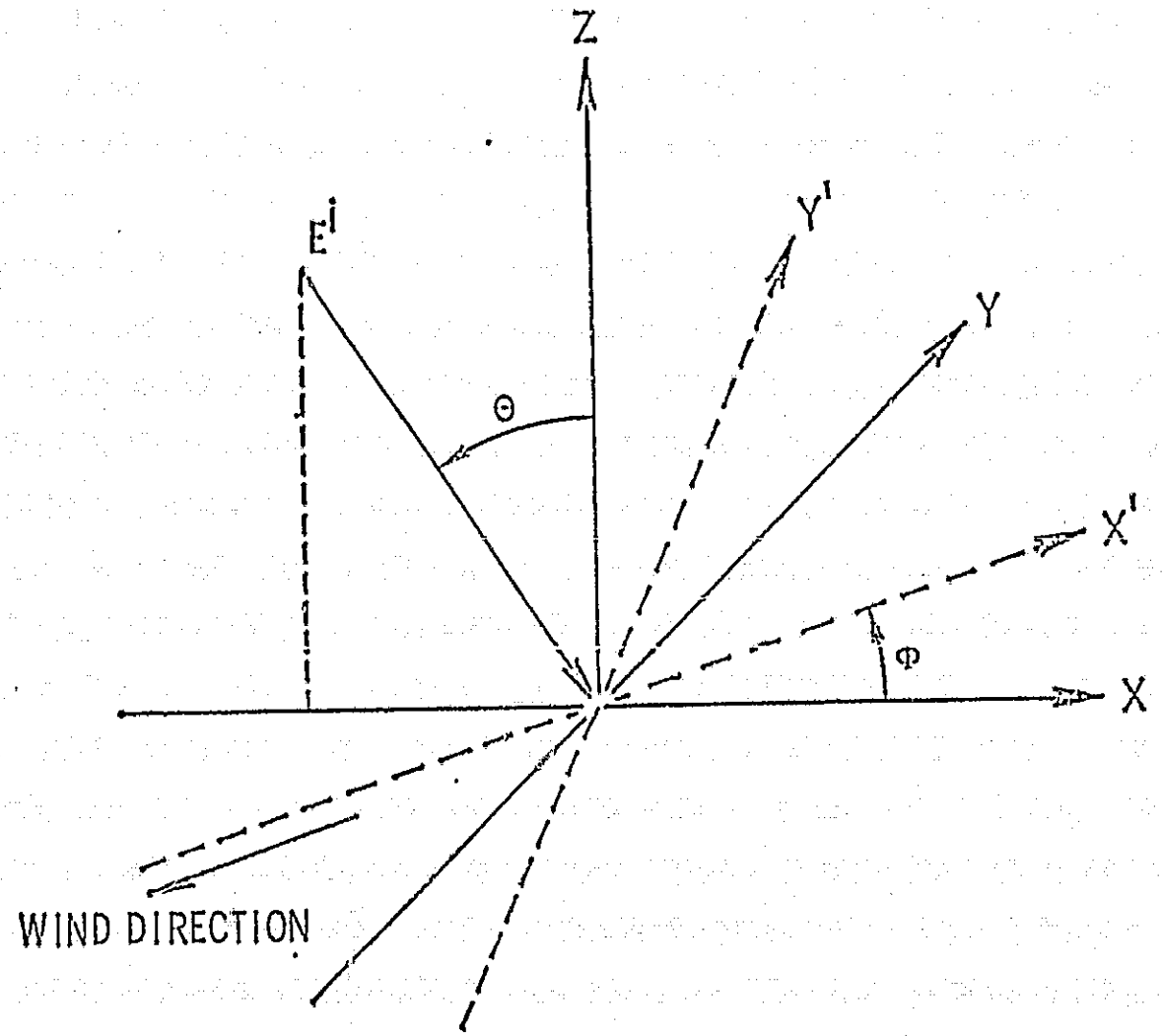

FIG 1 GEOMETRY OF THE SCATTER PROBLEM

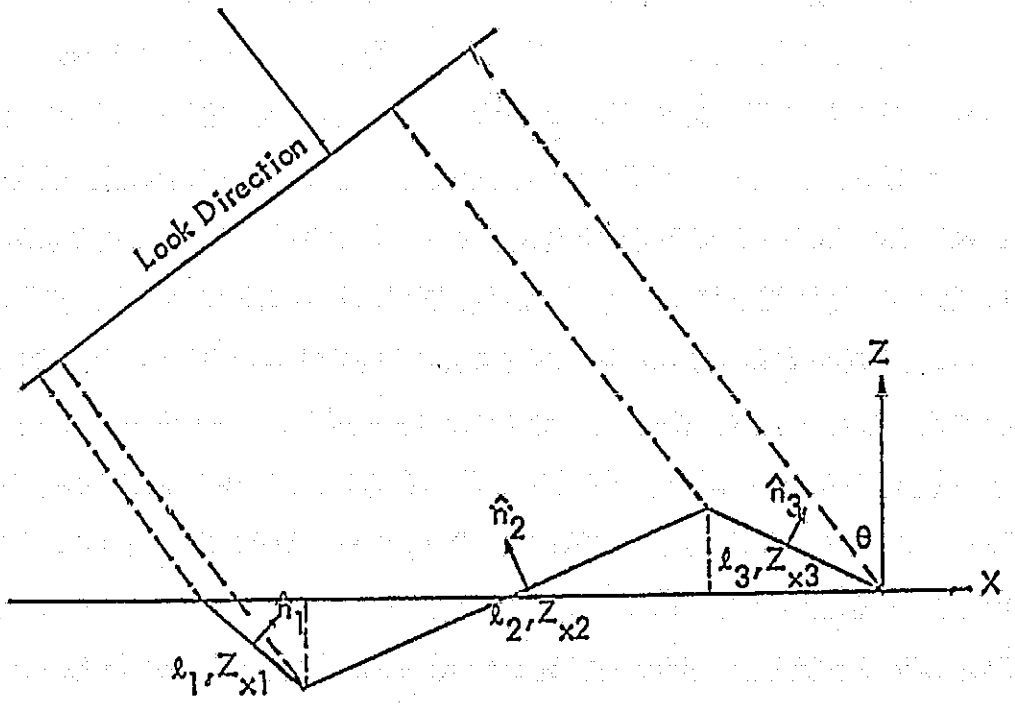

FIG 2 DIAGRAM ILLUSTRATING THE RELATION BETWEEN $P_o(Z_{x2})$ AND $P(Z_{x2})$

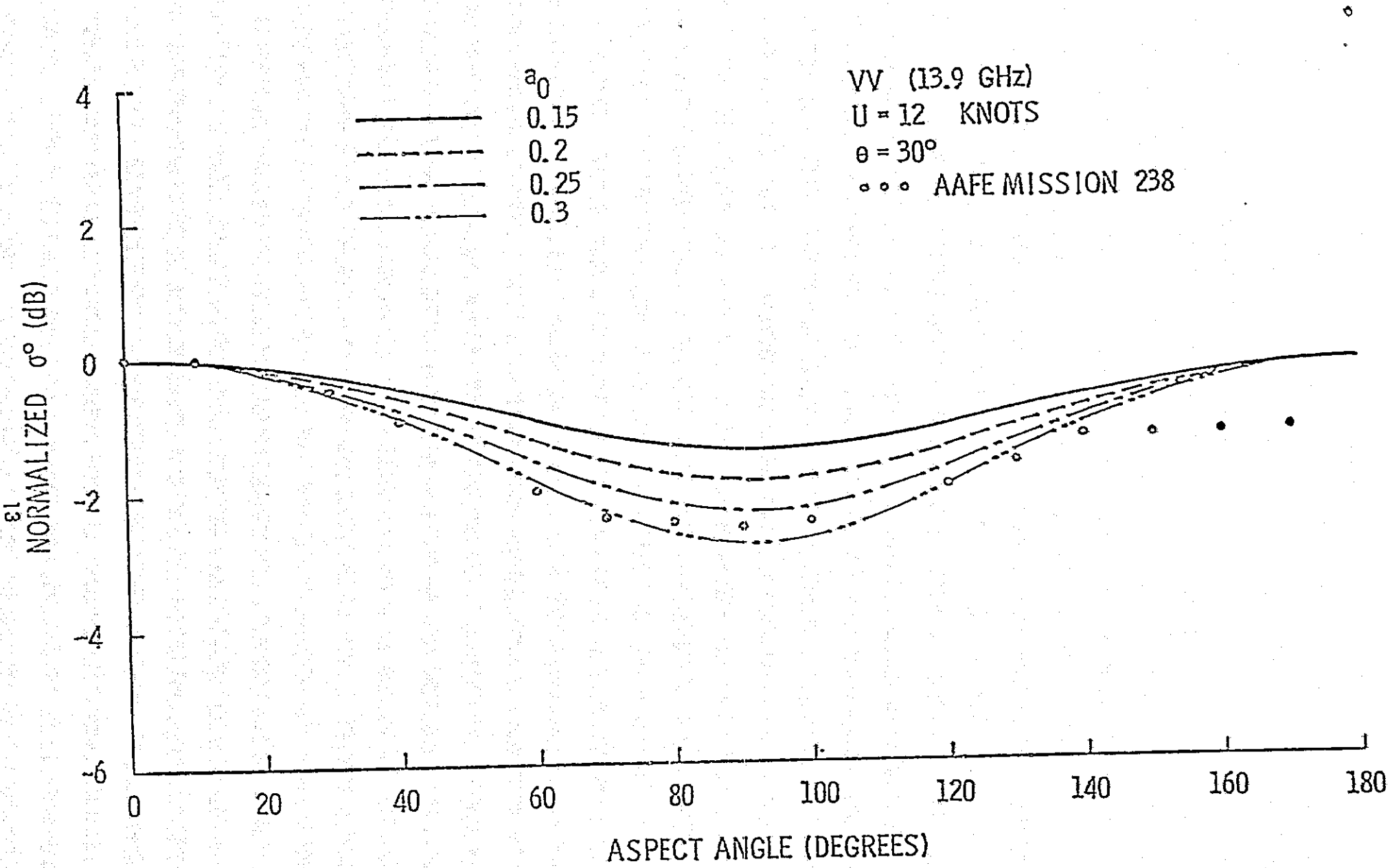

Figure 3α Azimuthal Dependence of σ° at $\theta=30^\circ$, U=12.0 Knots and 13.9 GHz for Various Choices of a_o for VV

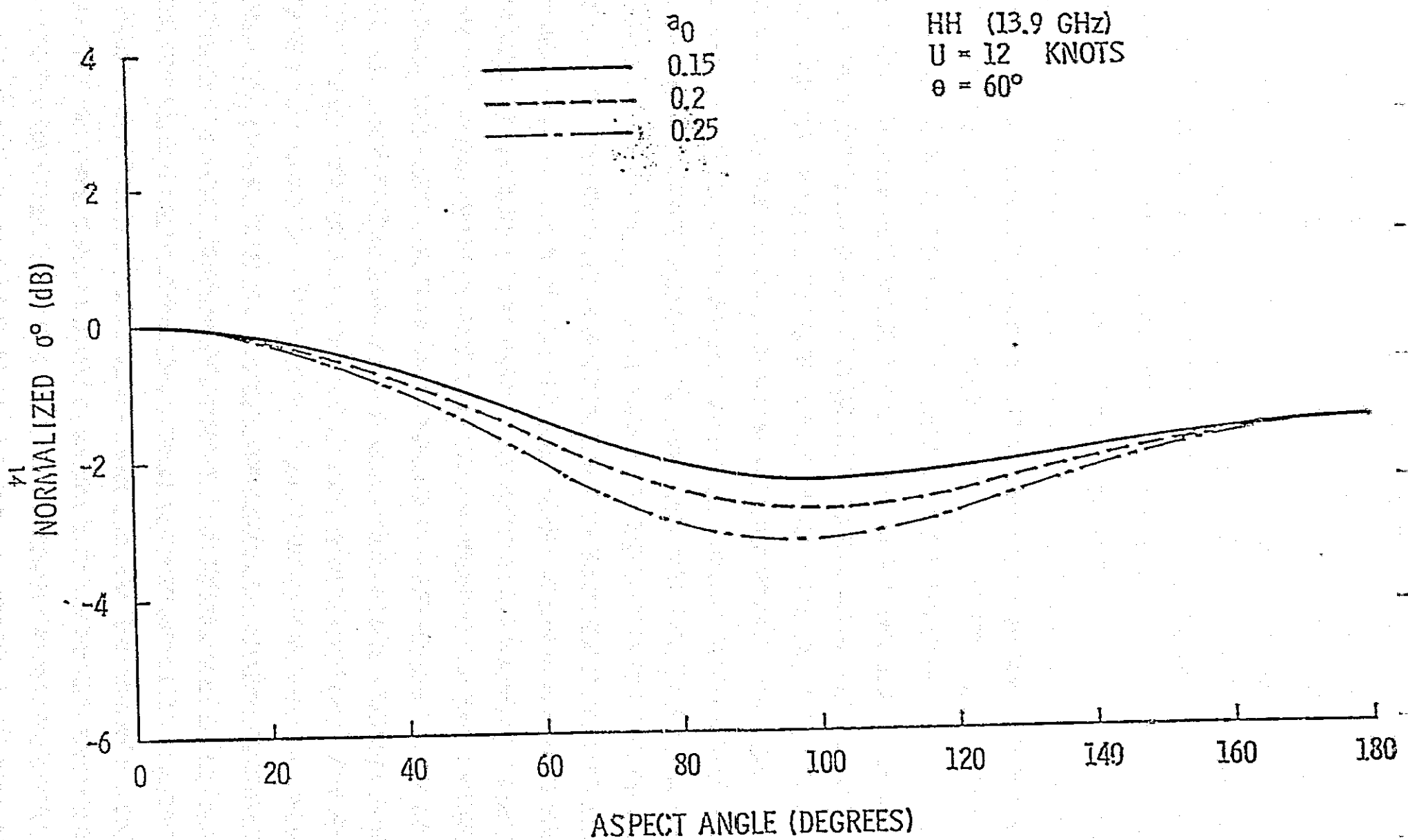

Figure 3b Azimuthal Dependence of σ° at $\theta=60^\circ$, U=12.0 Knots and 13.9 GHz for Various Choices of a_o for HH

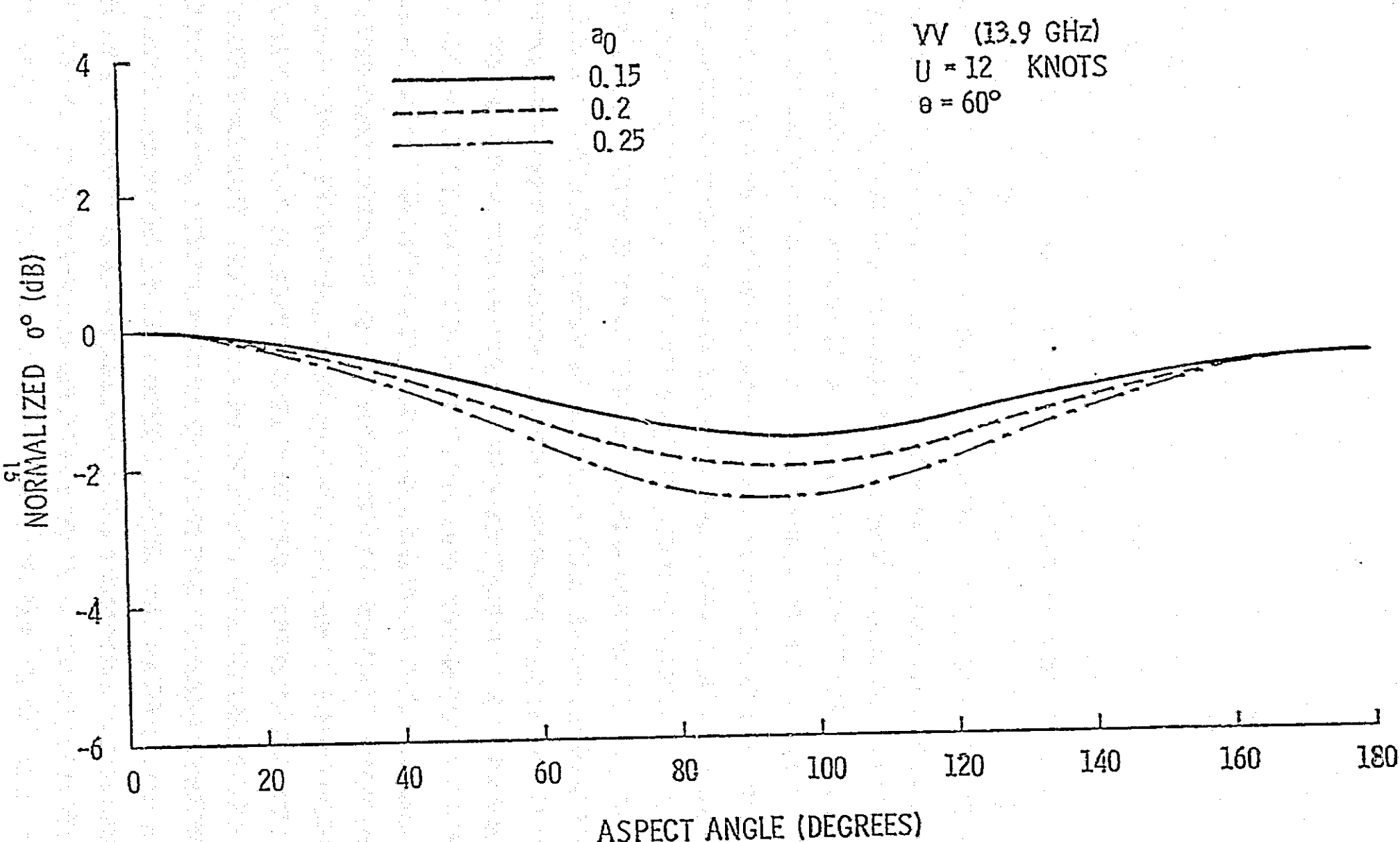

Figure 3c Azimuthal Dependence of σ° at $\theta=60^\circ$, U=12.0 Knots and 13.9 GHz for Various Choices of a_o for VV

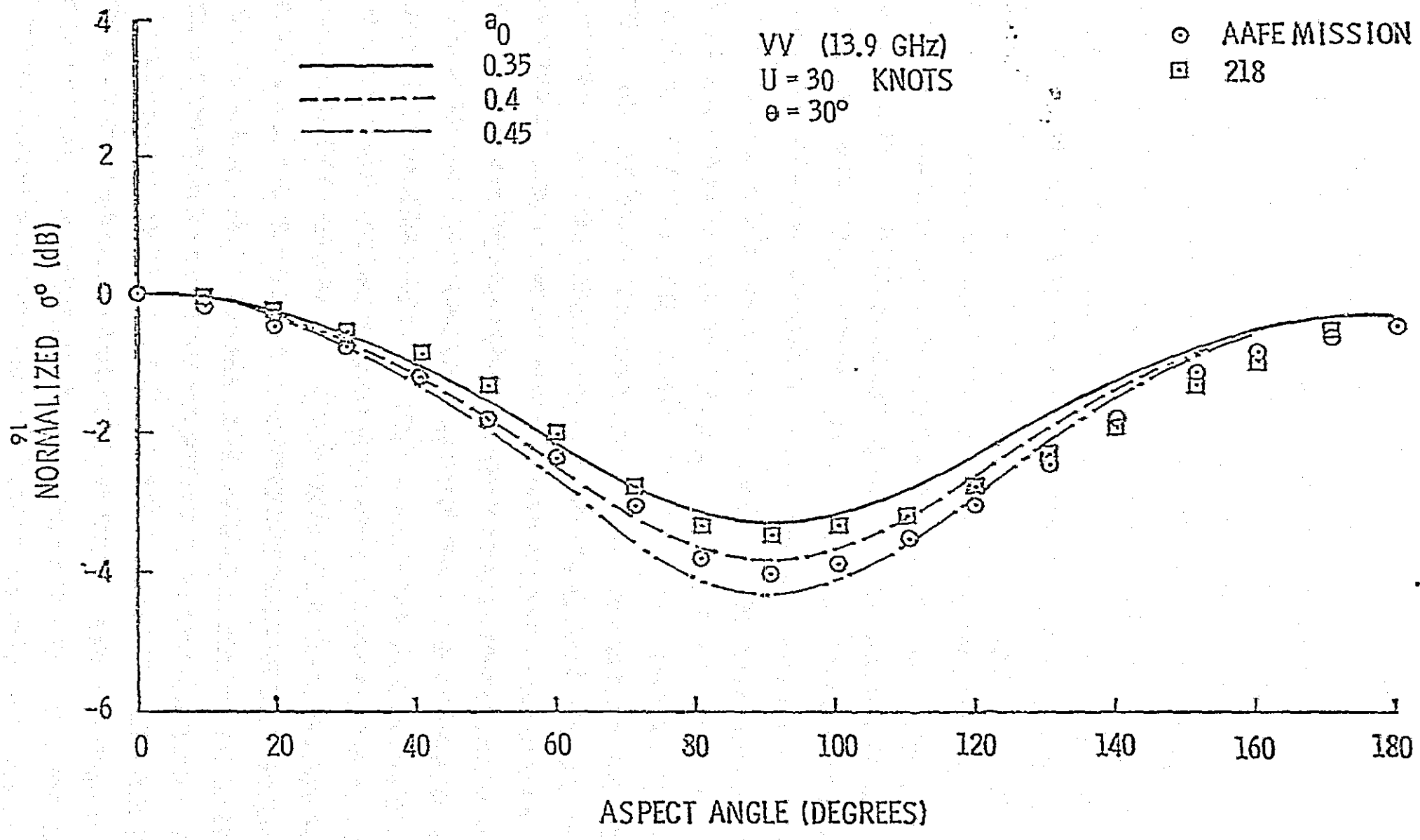

Figure 4a Azimughal Dependence of σ° at $\theta = 30^\circ$, U=30.0 Knots and 13.9 GHz for Various Choices of a_o for VV Together With AFEE Data Mission 218

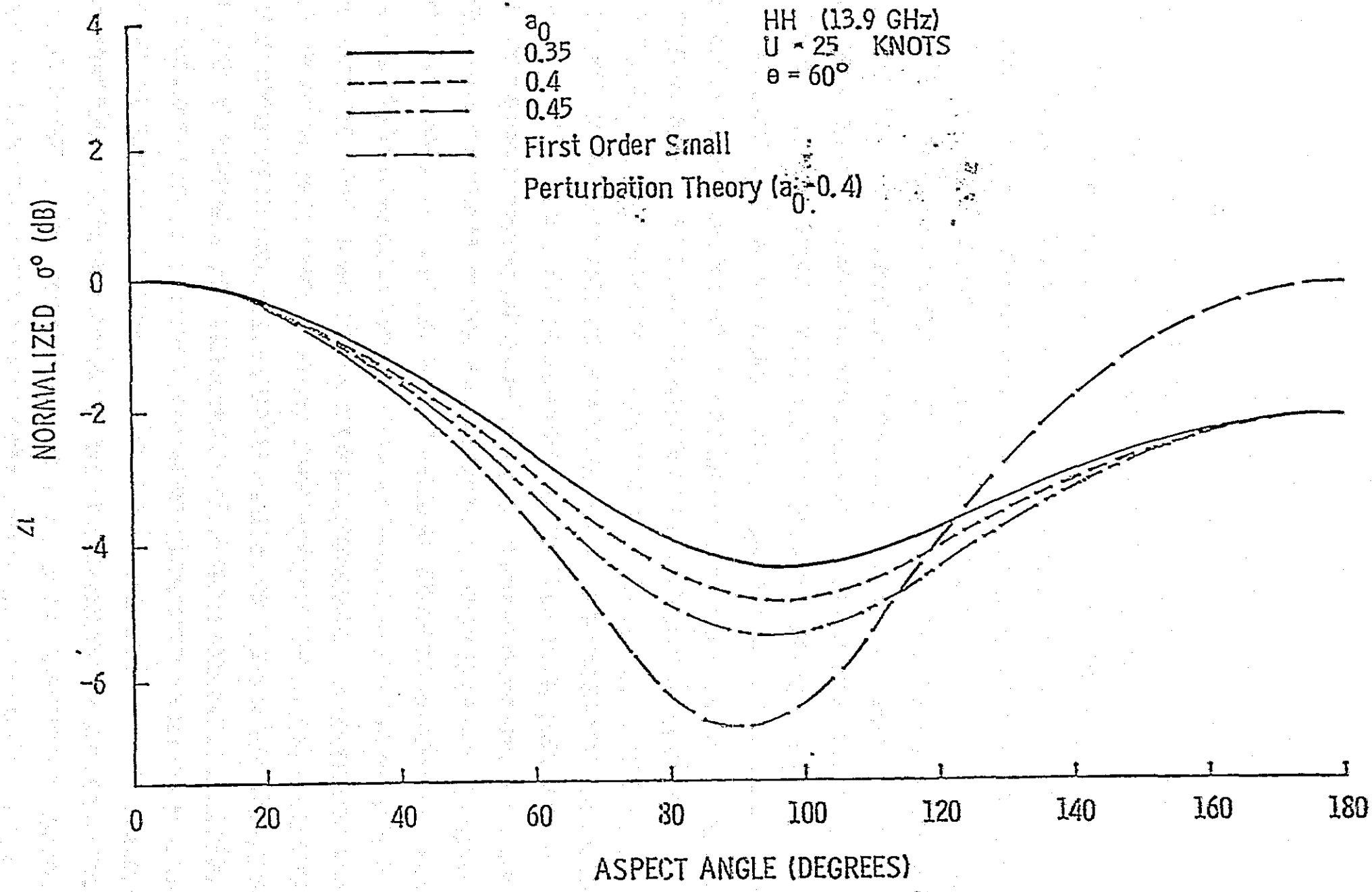

Figure 4b Azimuthal Dependence of σ° at $\theta=60^\circ$, U=25.0 Knots and 13.9 GHz for Various Choices of a_o for HH. The first order small perturbation results are also shown for comparison.

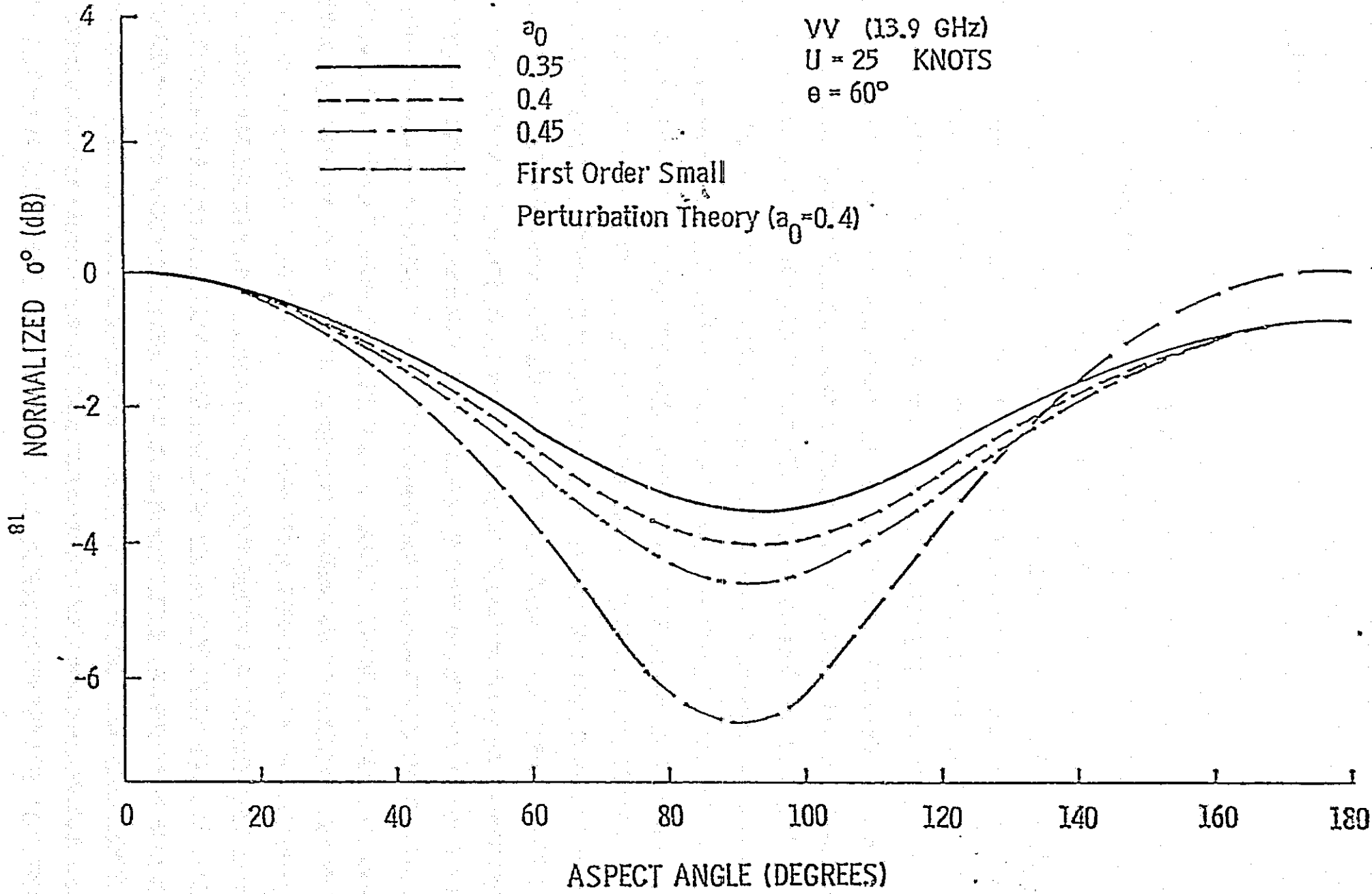

Figure 4c Azimuthal Dependence of σ° at θ=60°, U=25.0 Knots and 13.9 GHz for Various Choices of a_o for VV. The first order small perturbation results are also shown for comparison.

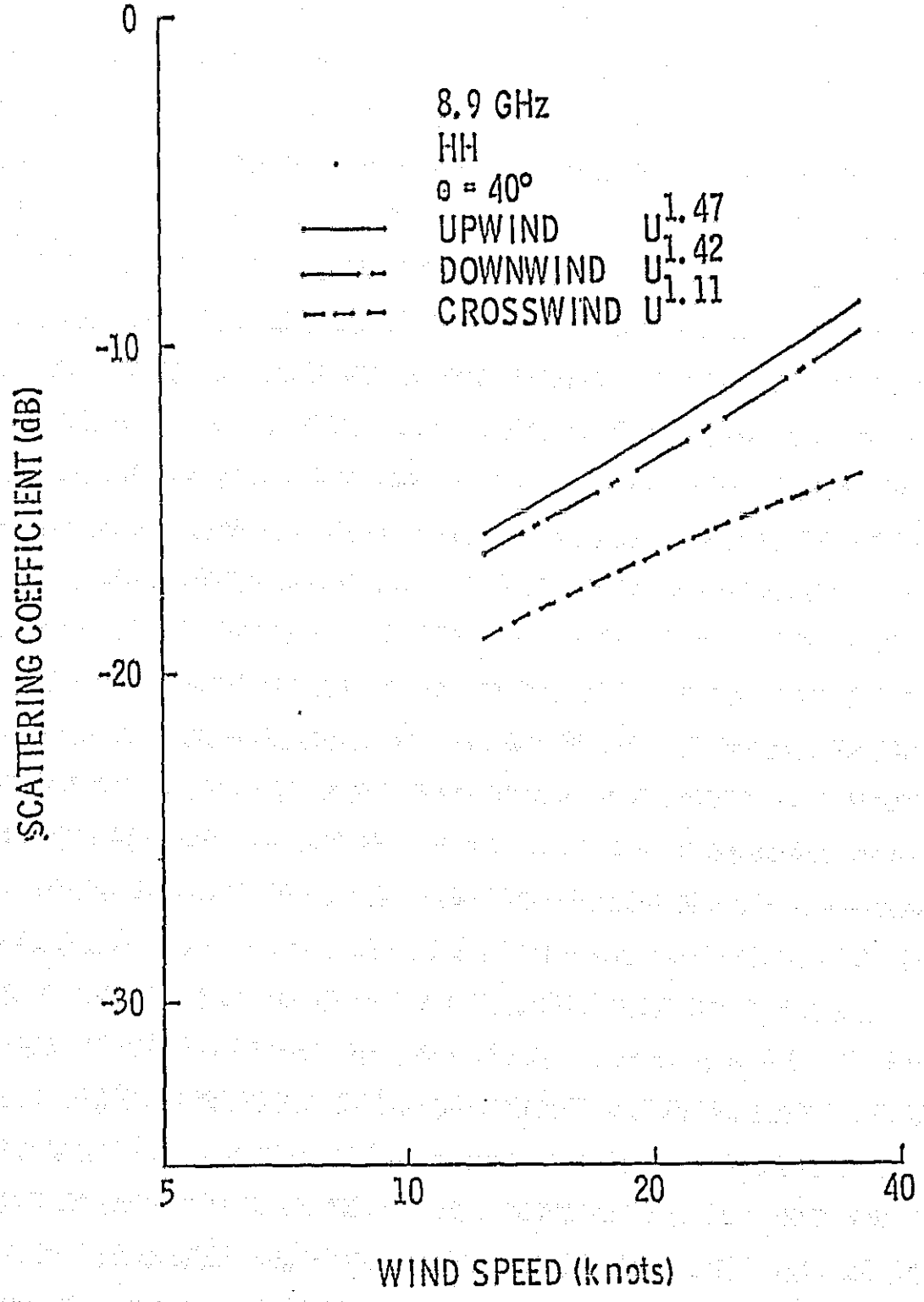

Figure 5a. Wind Dependence of σ^o at $\theta = 40^o$ and 8.9 GHz for HH

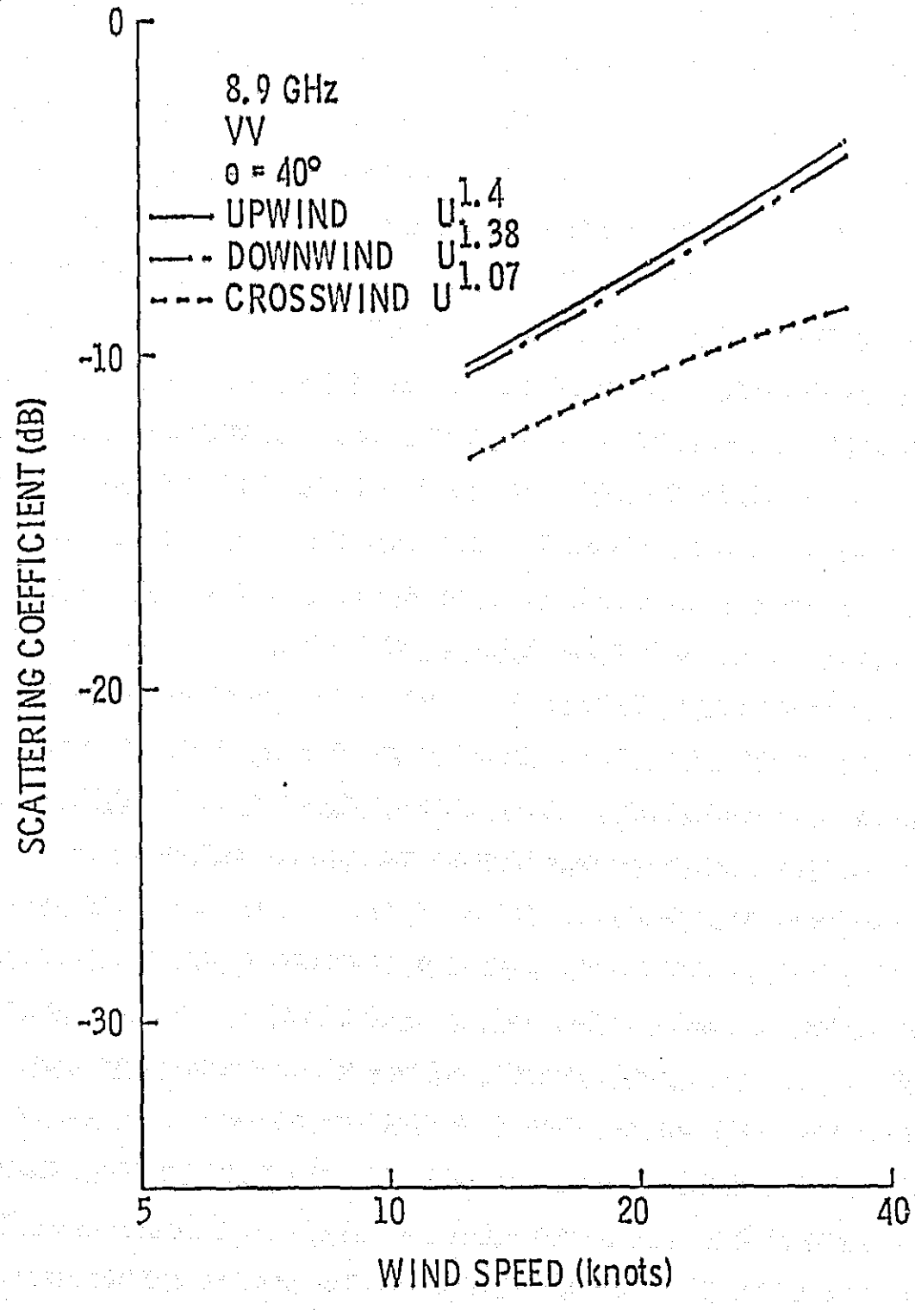

Figure 5b. Wind Dependence of σ^o at $\theta = 40^o$ and 8.9 GHz for VV

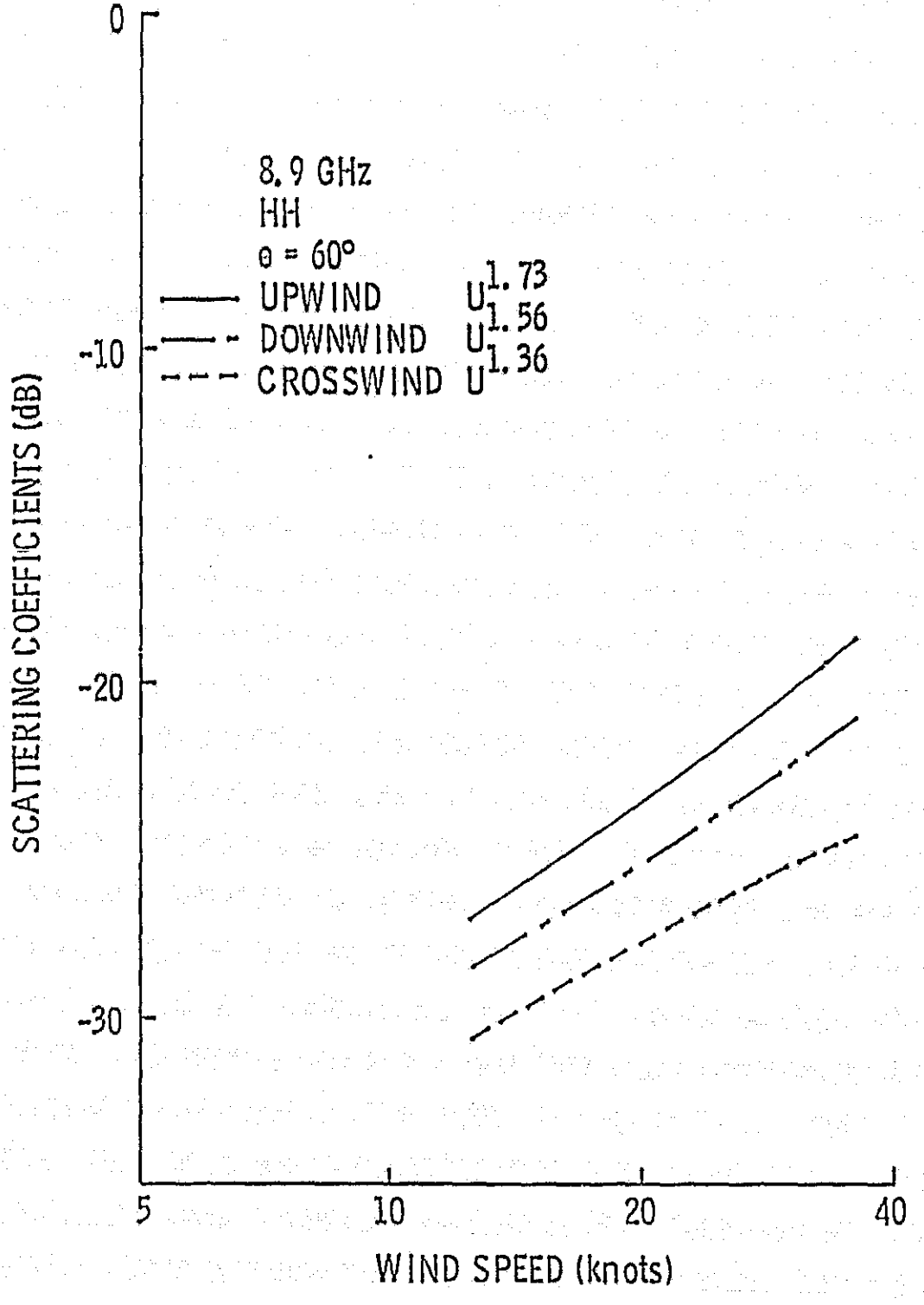

Figure 6a. Wind Dependence of σ^{o} at $\theta = 60^{o}$ and 8.9 GHz for HH

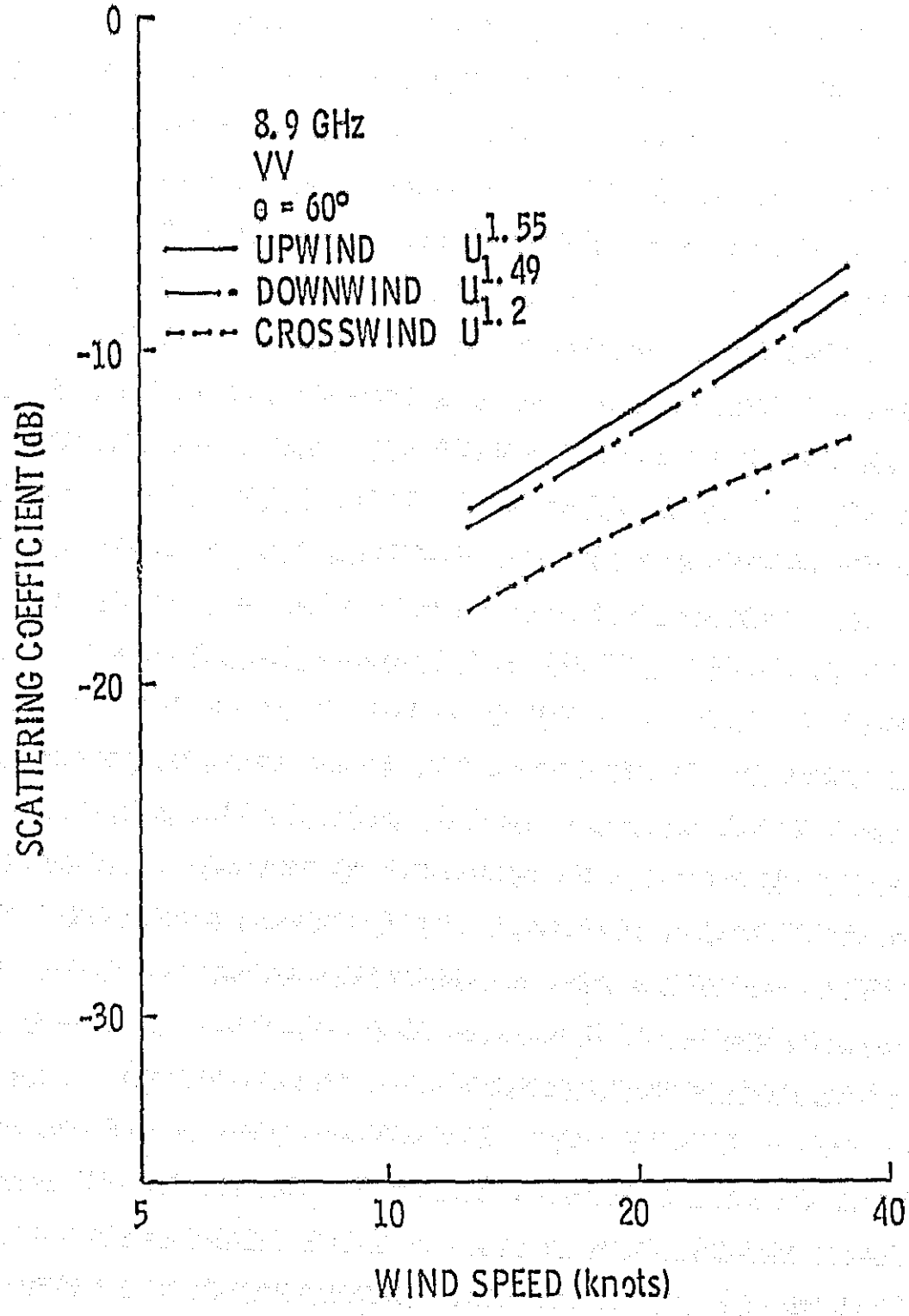

Figure 6b. Wind Dependence of σ° at $\theta = 60^{\circ}$ and 8.9 GHz for VV

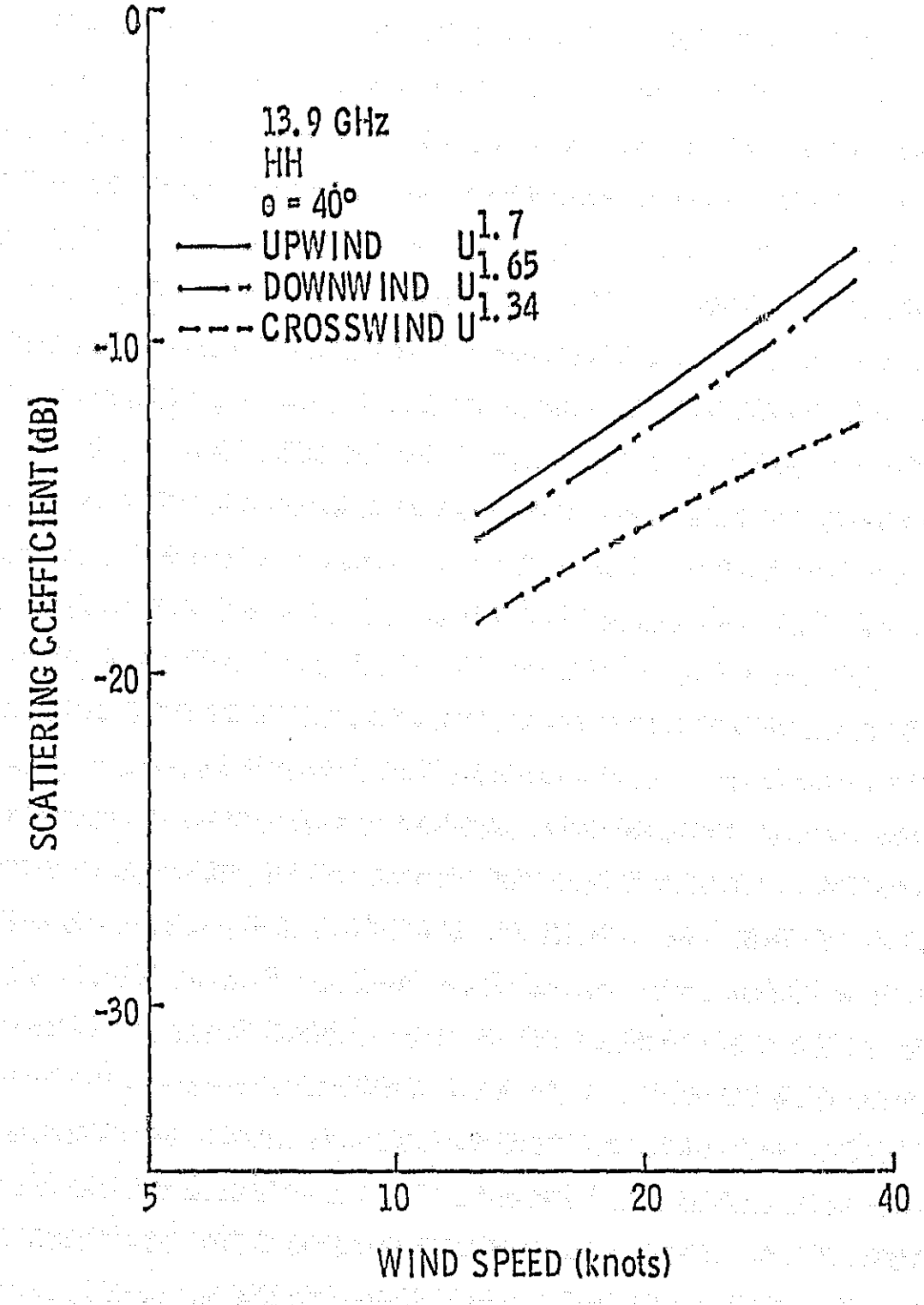

Figure 7a. Wind Dependence of σ^{o} at $\theta = 40^{o}$ and 13.9 GHz for HH

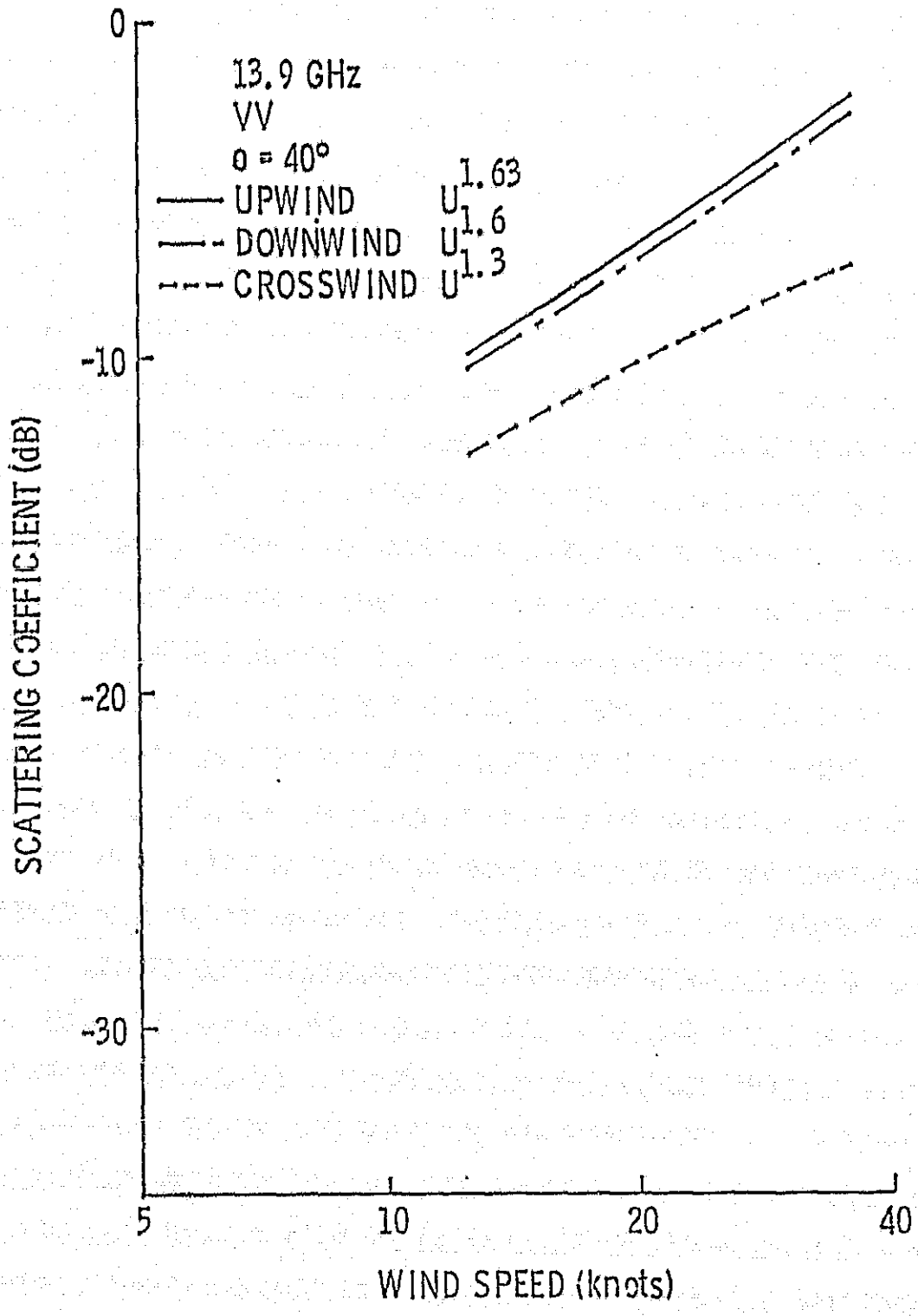

Figure 7b. Wind Dependence of σ^o at $\theta = 40^o$ and 13.9 GHz for VV

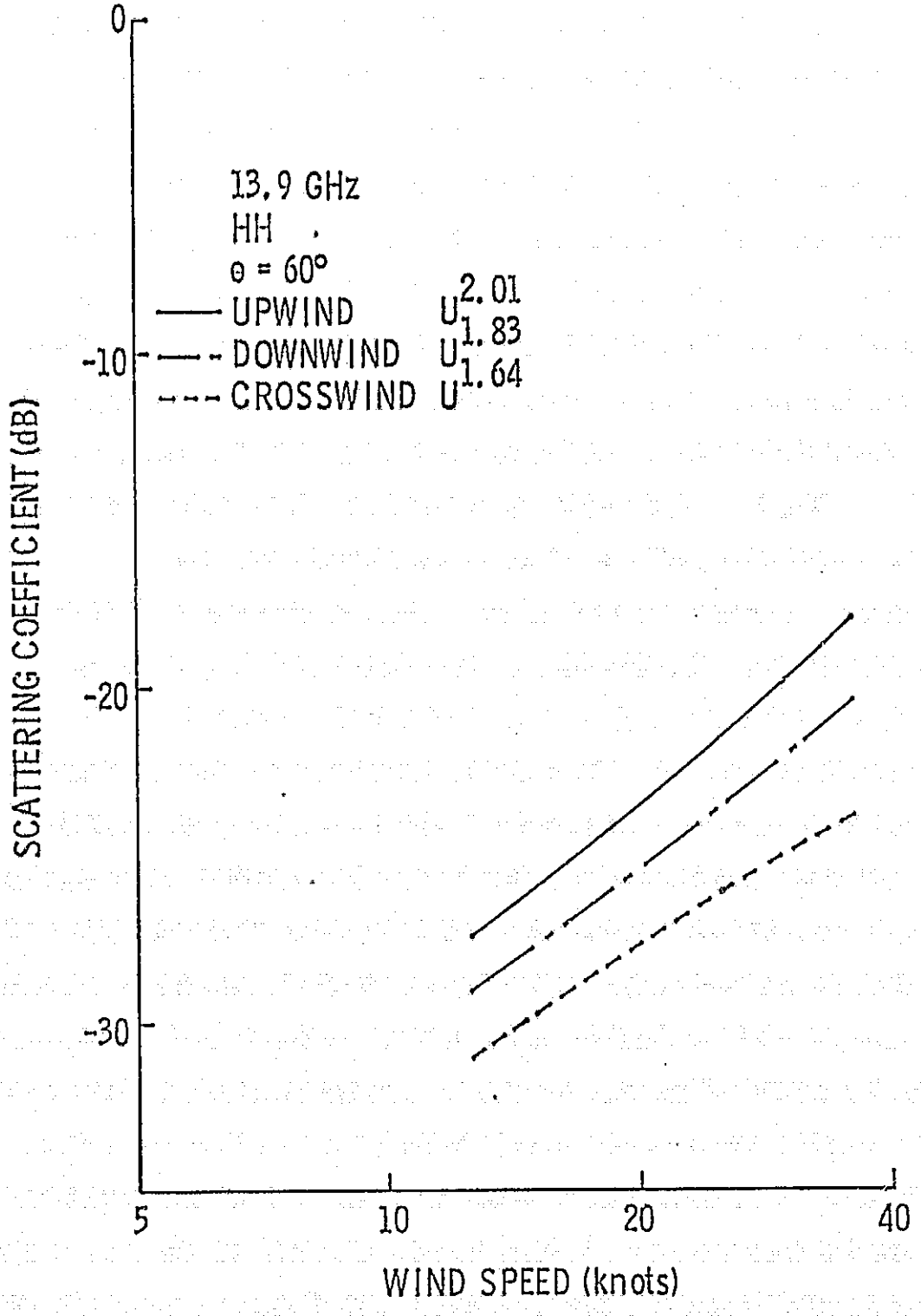

Figure 8a. Wind Dependence of σ^o at $\theta = 60^o$ and 13.9 GHz for HH

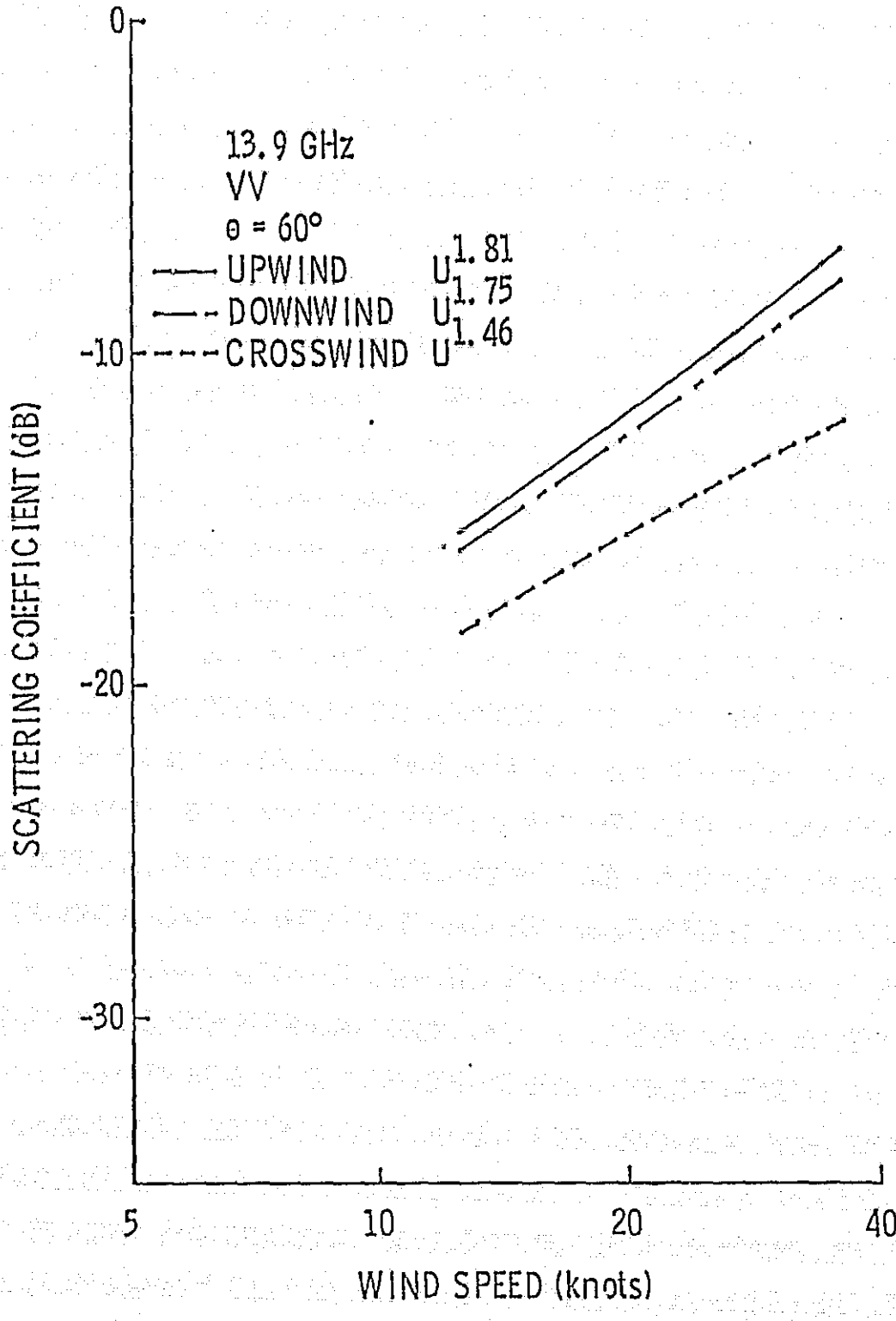

Figure 8b. Wind Dependence of σ^o at $\theta = 60^o$ and 13.9 GHz for VV